Author Manuscript

Author Manuscript

Author Manuscript

Author Manuscript

HHS Public Access

Author manuscript

Comput Biol Med. Author manuscript.

Analysis of speed, curvature, planarity and frequency characteristics of heart vector movement to evaluate the electrophysiological substrate associated with ventricular tachycardia

Larisa G. Tereshchenko, MD, PhD[1], **Jonathan W. Waks, MD**[2], **Muammar Kabir, PhD**[1], **Elyar Ghafoori, MS**[1], **Alexei Shvilkin, MD**[2], and **Mark E. Josephson, MD**[2]

[1]Knight Cardiovascular Institute, Oregon Health & Science University, Portland, OR

[2]Division of Cardiovascular Medicine, Beth Israel Deaconess Medical Center, Harvard Medical School, Boston, MA

Abstract

Background—We developed a novel method of assessing ventricular conduction using the surface ECG.

Methods—Orthogonal ECGs of 81 healthy controls (age 39.0±14.2 y; 51.8% males; 94% white), were compared with iDower-transformed 12-lead ECGs (both 1000 Hz), recorded in 8 patients with infarct-cardiomyopathy and sustained monomorphic ventricular tachycardia (VT) (age 68.0±7.8 y, 37.5% male, mean LVEF 29 ±12%). Normalized speed at 10 QRS segments was calculated as the distance traveled by the heart vector along the QRS loop in three-dimensional space, divided by $1/10^{th}$ of the QRS duration. Curvature was calculated as the magnitude of the derivative of the QRS loop tangent vector divided by speed. Planarity was calculated as the mean of the dihedral angles between 2 consecutive planes for all planes generated for the median beat. Orbital frequency (a scalar measure of rotation rate of the QRS vector) was calculated as a product of speed and curvature.

Results—Mixed regression analysis showed that speed was slower [6.6 (95%CI 4.4–8.9) vs. 24.6 (95%CI 11.5–37.7) μV/ms; P<0.0001]; orbital frequency was smaller [1.4 (95%CI 1.2–1.6) vs. 6.8 (95%CI 5.4–8.1) ms^{-1}; P<0.0001], and planarity was larger by 3.6° (95%CI 1.4°–5.8; P=0.002) in VT cases than in healthy controls. ROC AUC for orbital frequency was 0.940 (95%CI 0.935–0.944) across all frequencies and QRS segments. ROC AUC for planarity at 70–249 Hz was 0.995 (95%CI 0.985–1.00). ROC AUC for speed at 70–79Hz was 0.979 (95%CI 0.969–0.989).

© 2015 Published by Elsevier Ltd.

Correspondence: Larisa Tereshchenko, 3181 SW Sam Jackson Park Rd; UHN62; Portland, OR, 97239. tereshch@ohsu.edu. Phone: 503-494-7400; Fax: 503-494-8550.

Conflict of interest: none

Publisher's Disclaimer: This is a PDF file of an unedited manuscript that has been accepted for publication. As a service to our customers we are providing this early version of the manuscript. The manuscript will undergo copyediting, typesetting, and review of the resulting proof before it is published in its final citable form. Please note that during the production process errors may be discovered which could affect the content, and all legal disclaimers that apply to the journal pertain.

Author Manuscript Author Manuscript Author Manuscript Author Manuscript

Conclusion—This novel method reveals characteristic features of an abnormal electrophysiological substrate associated with VT.

Keywords

ventricular tachycardia; heart vector; conduction velocity; vectorcardiography

Introduction

Implantable cardioverter-defibrillators (ICDs) have been shown to reduce mortality in patients at risk for sudden cardiac death (SCD) due to life-threatening ventricular arrhythmias (ventricular tachycardia (VT) and ventricular fibrillation)[1]. Current risk stratification for primary prevention ICD implantation is based primarily on left ventricular ejection fraction (LVEF) and the presence of heart failure symptoms[2], but these factors have limited discriminatory value[3], and ICD implantation is not without risk[4]. It is therefore important to develop new, clinically meaningful, and mechanistically sound markers for an increased risk of ventricular arrhythmias, to allow identification of those individuals who would most benefit from prophylactic ICD implantation.

VT can, in theory, be cured by catheter based radiofrequency ablation. Successful VT ablation can improve survival and quality of life, minimize or even eliminate the need for ICD therapies and/or toxic antiarrhythmic drugs[5, 6], and decrease rates of heart failure (HF) hospitalizations. However, VT can recur after a successful ablation, even if aggressive ventricular stimulation is unable to re-induce VT at the end of the procedure[7]. Further improvement in detection and characterization of the electrophysiological (EP) substrate of VT is needed for accurate risk stratification of patients at risk of VT, and for development of an objective end-point of VT ablation. In this manuscript, we present a novel method for detection and quantification of an abnormal EP substrate.

Methods

We used a novel method to compare properties of ventricular conduction in healthy individuals and patients with post-myocardial infarction (MI) scar and sustained monomorphic VT (MMVT), undergoing VT ablation.

Study population: healthy individuals

We retrospectively analyzed de-identified digital electrocardiograms (ECGs) from the Intercity Digital Electrocardiogram Alliance (IDEAL) study[8]. This study enrolled a cohort of healthy participants of both genders and a wide age distribution. Digital ECGs were provided by the Telemetric and Holter ECG Warehouse[9]. Details of the IDEAL study population have been previously characterized by our group[10, 11], and by others[8]. Only IDEAL participants 18 years and older were included in the present analysis. All IDEAL study participants provided informed consent prior to enrollment.

We included 81 IDEAL study participants in this analysis. No patients had a history of MI or other cardiovascular disease. The mean age of participants was 39.0±14.2 y (range 19–82 y). Both genders were equally represented: 42 males (51.8%) and 39 females (48.2%). Most

Author Manuscript Author Manuscript Author Manuscript Author Manuscript

participants were white (n=76; 94%). Mean systolic blood pressure was 116.5±11.4 mmHg and mean diastolic blood pressure was 75.4±8.0 mmHg. Mean body mass index was 24.6±5.5 kg/m^2. Mean heart rate was 64.9±11.0 bpm. Mean QRS duration was 95±7 ms. No patients had fascicular block or complete bundle branch block.

Study population: patients with post-MI scar and MMVT undergoing VT ablation

A retrospective study of patients undergoing VT ablation was approved by the Beth Israel Deaconess Medical Center (BIDMC) Institutional Review Board. For this proof of concept study we analyzed the data of 8 patients (mean age 68.0±7.8 y, 37.5% male) with prior MI, and infarct-related cardiomyopathy (mean LVEF 29±12%), and multiple episodes of sustained MMVT who were referred to BIDMC for VT ablation.

ECG data asquisition and analysis

IDEAL study participants underwent 10 minutes of continuous orthogonal (XYZ) ECG recording at rest via the SpaceLab-Burdick digital Holter recorder (SpaceLab-Burdick, Inc., Deerfield, WI) with 1000 Hz sampling frequency and 4.88 μV amplitude resolution. Five consecutive sinus beats were included in the analysis.

In the post-MI/MMVT patients, a standard 12-lead ECG obtained prior to ablation was continuously recorded and saved on the GE Prucka CardioLab EP System (Wipro GE Healthcare, Milwaukee, WI). Raw, high-resolution, digital 12-lead ECG signals (1000 Hz sampling frequency, 1 μV amplitude resolution) were extracted and transformed into orthogonal XYZ ECG leads using the inverse Dower transformation[12].

Step 1. Detection of the origin of VCG loops for each cardiac cycle—The origin point of each cardiac cycle/VCG loop was detected as previously described[11] by defining the mid-point along the line connecting the two points (defined as P1 and P2) that were closest in space but significantly separated in time (Figure 1A).

Step 2. Removal of respiration effects—The effect of respiration on VCG loops was then removed utilizing an approach developed by Sornmo and associates[13, 14]. First, VCG loops were aligned in space (Figure 1B) and the origin point was determined. All loops were then translated in space to an arbitrary point (defined as (0,0,0)) so that the origin point of each VCG loop was located at the same point in three-dimensional space. VCG loops were then rotated and further aligned so that the lines connecting points P1 and P2 for each VCG loop were all in the same plane. For further removal of respiratory effects, each individual VCG loop was re-scaled by a factor which was calculated as the ratio of the mean VCG loop for all beats divided by the each individual VCG loop[13, 14] (Figure 1C).

Step 3. Detection of the onset and offset of VCG loop components (P, QRS, T, and U loops)—The onset and offset of the P, QRS, T, and U loops were identified by searching the P1and P2 points using a window around respective spatial vector component (P, QRS, T, and U loops). Specifically, to determine the onset/offset of the QRS loop, search was performed using a window around the peak of the spatial QRS vector (Figure 1D and Supplemental Figure 1).

Author Manuscript Author Manuscript Author Manuscript Author Manuscript

Step 4. Measurement of the speed, curvature, and planarity of the heart vector movement during ventricular depolarization—Each QRS loop was divided into 10 equal segments. To calculate the speed of heart vector movement during the each QRS segment, the distance traveled by the heart vector along the QRS loop during each of the 10 segments was measured in three-dimensional space, and divided by $1/10^{th}$ of the QRS duration.

Curvature, a measure of how much the VCG loop deviated from a straight line at a given point was calculated as follows:

$$curvature = \frac{\boldsymbol{T}'(t)}{\boldsymbol{r}'(t)}$$

Where $\boldsymbol{r'}(t)$ is the derivative of the 3-dimensional VCG loop (defined by the time parameterized function $\boldsymbol{r}(t) = \langle x(t), y(t), z(t) \rangle$ at time t, and $\boldsymbol{T'}(t)$ is the derivative of the unit tangent vector $\boldsymbol{T}(t)$ at time t. The average curvature across each QRS segment was used for analysis. Figure 2 and supplemental movies illustrate heart vector velocity and curvature, plotted for 5 consecutive sinus beats.

Orbital frequency, a scalar measure of rotation rate of the QRS vector, was calculated as a product of velocity and curvature, averaged over each QRS segment. Orbital frequency is a scalar measure of rotation rate of the QRS vector.

Planarity θ (theta) was calculated as the mean of the dihedral angles between two consecutive planes for all planes generated for the median beat. Starting from the onset of the QRS loop, each plane was generated using 3 sample points of the QRS vector in three-dimensional space. Each of these 3 points were subsequently shifted to generate consecutive planes. The dihedral angles between each two consecutive planes were calculated for each beat and subsequently averaged.

Step 5. Filtering of VCG loops—Filtering of VCG loops was then performed with a 10 Hz bandpass filter incrementally at 10–19Hz, 20–29Hz, 30–39Hz, 40–49Hz, 50–59Hz, 61–69Hz, 70–79Hz, 80–89Hz, 90–99Hz, 100–109Hz, 110–119Hz, and 70–249Hz. Of note, 60Hz was excluded from our analysis to minimize confounding due to power-line interference. Supplemental movie shows QRS loops filtered at various bandpass frequencies.

Step 6. Measurements of velocity and curvature of filtered heart vector movement—Steps 3–4 were repeated at each bandpass frequency in order to measure speed, curvature, and planarity of filtered VCG loops.

Statistical analysis

Statistical analysis was conducted using Stata 13 (StataCorp, College Station, TX). All normally distributed continuous variables were presented as mean and standard deviation. Normally distributed numerical variables in healthy subjects and patients with post-MI MMVT were compared using a standard t-test. Curvature was log-transformed to normalize

Author Manuscript Author Manuscript Author Manuscript Author Manuscript

its distribution prior to statistical analyses. In order to appropriately account for the correlations induced by the clustered data structure (speed/curvature measured at 10 time segments within QRS, at 13 different frequency bands), we constructed multilevel mixed regression models to determine the strength of associations of the speed/curvature with patient substrate (healthy vs. MI/MMVT cases). Area under the receiver operating characteristic (AUC ROC) was used to test discrimination performance of speed, curvature, orbital frequency, and planarity across each QRS frequency.

Results

Comparison of QRS VCG loop speed in healthy participants and patients with MI and MMVT

Supplemental movie files show QRS VCG loops for 5 consecutive sinus beats (unfiltered and with all bandpass filters) in a representative healthy IDEAL study participant and a patient with MMVT. The speed of heart vector movement in each QRS segment and at each frequency band in healthy IDEAL participants and patients with post MI MMVT is shown in Supplemental Table 1 and Figure 3. In healthy participants, the QRS loop was characterized by relatively slow initial speed followed by rapid conduction making up the majority of the QRS loop, maximum speed at the midpoint of the QRS, and relatively slow speed in the terminal portion of the QRS loop. Mixed regression analysis showed that across all QRS segments and across all filtering frequencies, speed was significantly slower in VT cases than in healthy controls [6.6 (95% CI 4.4–8.9) vs. 24.6 (95% CI 11.5–37.7) μV/ms; P<0.0001]. The difference in speed between these 2 groups was especially striking in the 5^{th}, 6^{th}, and 7^{th} segments. In comparison to healthy controls, maximum speed in VT patients occurred in the first third of the QRS (Figure 3). Mixed regression analysis demonstrated that each 10 μV/ms decrease in velocity was associated with a 41% increase in odds of being in the post MI/MMVT group (OR 1.41; 95% CI 1.34–1.49; P<0.0001). Post-estimation AUC ROC for speed across all QRS segments and frequencies was 0.923 (95% CI 0.900–0.946). Speed filtered at 70–79 Hz, 61–69Hz, and 50–59 Hz demonstrated the best accuracy for discrimination between healthy controls and patents with prior MI and MMVT (Table 1).

Comparison of QRS VCG loop curvature in healthy participants and patients with MI and MMVT

A comparison of QRS loop curvature in healthy IDEAL participants and patients with MMVT at each frequency band is reported in Supplemental Table 2 and Figure 4. In healthy controls, QRS curvature was inversely related to QRS speed, with the minimum curvature observed at the time of the fastest QRS vector movement. A direct correlation between velocity and curvature was observed in VT patients (Figure 5).

Mixed regression analysis showed that across all QRS segments and all range of frequencies, curvature was smaller in VT cases than in healthy controls [1.8 (95%CI 1.0–2.5) vs. 3.0 (95%CI −0.3 – 6.4) μV^{-1}; P=0.002]. In mixed model regression, smaller curvature was associated with slightly higher odds of being in VT group: lower by a one unit, log-transformed curvature was associated with 7% higher odds of being in the VT group (OR 1.07; 95% CI 1.03 to 1.12; P=0.001). Post-estimation ROC AUC for curvature

Author Manuscript Author Manuscript Author Manuscript Author Manuscript

was modest overall (ROC AUC 0.579; 95% CI 0.562–0.595). The discrimination ability of curvature was inferior to that of speed (Table 1).

Comparison of QRS VCG loop orbital frequency in healthy participants and patients with MI and MMVT

Orbital frequency across all QRS segments and all frequency bands (Figure 6) was significantly higher in healthy controls compared to patients with MMVT [6.8 (95% CI 5.4–8.1) vs. 1.4 (95% CI 1.2–1.6) ms^{-1}; P<0.0001]. In a mixed regression analysis, one square root –transformed unit of orbital frequency was associated with nearly twice higher odds of being in the MMVT group (OR 1.86; 95% CI 1.84–1.89; P<0.0001). Post-estimation ROC AUC for orbital frequency was very high: 0.940 (95% CI 0.935–0.944). The discrimination ability of orbital frequency was especially high at high filtering frequencies (Table 1).

Variations in ventricular conduction in healthy participants and patients with MI and MMVT

Filtered QRS ***loops*** revealed ***prominent*** beat-to-beat variation in ventricular conduction in VT patients, but not in healthy ***controls*** (Figure 5 and supplemental movies). In patients with MI and MMVT bandpass filtering of the QRS VCG loop revealed variable ***beat-to-beat*** conduction which was not seen by looking at the QRS complex on the surface ECG.

Comparison of QRS VCG loop planarity in healthy participants and patients with MI and MMVT

One of the most striking differences between healthy controls and patients with MMVT was related to how QRS loops rotated within multiple planes (see supplemental movies). In healthy controls, QRS loops rotated predominantly in a single plane, but in patients with MI and MMVT, QRS loops rotated through multiple planes, forming a “cloud”. Mixed regression analysis demonstrated that, across all frequencies, (Figure 7) averaged planarity was larger in the MMVT group by 3.6° (95% CI 1.4°–5.8); P=0.002. A 10° increase in planarity averaged across all frequencies was associated with twice the odds of being in the MMVT group (OR 2.0; 95% CI 1.25–3.11; P=0.003). The discriminative ability of the planarity angle was especially high at 10–19, 20–29, and 70–249 Hz (Table 1).

Discussion

In this manuscript we presented a novel method using filtered VCG loops to visualize and quantify features of ventricular conduction which are inapparent on a standard 12-lead ECG in sinus rhythm. We described the key differences between normal ventricular conduction, and ventricular conduction in patients with prior MI and a substrate favorable for ventricular arrhythmias. We demonstrated that measurement of speed, curvature, orbital frequency and planarity angle of the heart vector movement throughout the QRS is possible, meaningful, and can discriminate between healthy controls and patients with prior MI and MMVT.

It is important to emphasize that we analyzed the QRS velocity vector magnitude which may not be representative of true intramyocardial conduction velocity (which cannot be measured non-invasively using the surface ECG). However, our results suggest that the heart vector movement throughout the QRS VCG loop may provide a non-invasive, quantifiable, and

Author Manuscript Author Manuscript Author Manuscript Author Manuscript

meaningful surrogate for intramyocardial conduction velocity, with multiple areas of slow and variable conduction in VT patients which are not present in healthy controls. Although this method of observing ventricular conduction which is inapparent on the surface ECG (inapparent ventricular conduction (IVC) method) requires further study and validation, once refined, it might be able to identify individuals at increased risk for VT and SCD, advance our understanding of VT mechanisms, and allow development of an objective, quantitative, and operator-independent end-point for VT ablation.

Slow conduction and areas of block within post-MI scar is a well-known cause of reentrant VT, and several methods have been developed to capture and quantify the presence of slow ventricular conduction associated with abnormal EP substrate. Signal-averaged ECG (SAECG) was developed to detect and quantify late potentials which are generated when ventricular tissue is activated later than usual towards the end of QRS complex[16]. The SAECG has demonstrated some value in risk stratification for SCD[17, 18], however, many post-MI scars (especially those due to anterior MI) have abnormal slow conduction which occurs early on within the QRS, and this type of abnormal conduction would be missed by a standard SAECG[19]. Attempts to refine the SAECG have been made[20, 21] and analysis of R-wave heterogeneity, which was developed[22] to quantify beat-to-beat heterogeneity in ventricular conduction, has also been associated with VT.

We have taken an entirely different approach. Our IVC-method measures velocity, curvature, orbital frequency, and planarity of the QRS VCG loop at different time points throughout the entire period of ventricular depolarization, and it therefore is able to assess inter- and intra-beat heterogeneity of ventricular conduction throughout the entire QRS complex. Scanning the QRS with narrow frequency (10 Hz) band-passes allows us to further highlight subtle abnormalities and variations in ventricular conduction at any point of the cardiac cycle. We believe our method may be especially helpful for describing variation in ventricular conduction in different types of fibrosis (compact, patchy, interstitial, and diffuse)[23]. Further studies using and validating the IVC-method, however, are needed to test this hypothesis. The methodology used for evaluating speed, curvature, orbital frequency, and planarity in the QRS loop can be extended to other VCG loops (P, T, and U loops) as well.

Limitations

Surface orthogonal XYZ ECGs, which reflect the dipolar XYZ vectorial components of the spatial vector representing depolarization and repolarization of the entire myocardium, were analyzed in this study. Patients with post-MI scar and MMVT may have significant non-dipolar components which are better identified using body surface potential maps, rather than surface ECG. Nevertheless, this method demonstrated high discrimination abilities for detection of abnormal EP substrate in patients with MMVT. Utilization of easily available surface ECGs is another advantage of this method.

Conclusions

We present a novel method of assessing EP substrate by measuring speed, curvature, orbital frequency, and planarity of filtered, three-dimensional VCG loops. Normal ventricular

Author Manuscript Author Manuscript Author Manuscript Author Manuscript

conduction is characterized by movement of the heart vector through a nearly single plane across all frequencies, maximum QRS loop speed mid-QRS, and an inverse relationship between QRS loop speed and curvature.

Ventricular conduction in post-MI patients with MMVT is characterized by remarkably slower speed than in healthy participants, the presence of a relatively slow conduction in the middle of the QRS complex, rotation of filtered QRS loops through numerous planes resulting in a spherical “cloud” of filtered QRS loops, a direct relationship between speed and curvature, low orbital frequency, and prominent beat-to-beat heterogeneity of ventricular conduction at filtering frequencies ≥20 Hz. Analysis of the speed, curvature, orbital frequency, and planarity of filtered QRS VCG loops permits characterization of ventricular conduction which is inapparent on the surface ECG. Further study of the IVC method is needed to determine its value as a risk stratification tool for VT and SCD, and as an objective end-point to determine the “success” of VT ablation.

Summary

In this work we present a novel method of visualizing and quantifying inapparent features of ventricular conduction by measuring speed, curvature, orbital frequency, and planarity of the filtered heart vector movement in the QRS VCG loop and characterizing intra- and inter-beat heterogeneity of this conduction.

Normal ventricular conduction is characterized by movement of the heart vector thru a single plane across all frequencies, maximum QRS VCG loop speed mid-QRS, high orbital frequency, and an inverse relationship between QRS VCG loop speed and curvature.

Ventricular conduction in patients with prior MI and MMVT is characterized by remarkably slower speed than in healthy participants, the presence of slow conduction in the middle of the QRS, low orbital frequency, rotation of filtered QRS loops through numerous planes resulting in a spherical “cloud” of filtered QRS loops, a direct relationship between speed and curvature, and beat-to-beat heterogeneity of ventricular conduction. Further study of this novel method is needed to validate its value in the characterization of EP substrate and as a risk stratification tool for VT and SCD.

Supplementary Material

Refer to Web version on PubMed Central for supplementary material.

Acknowledgments

Funding Sources:

This research was supported in part by the National Institute of Health #1R01HL118277 (LGT and MEJ).

References

1. Epstein AE, DiMarco JP, Ellenbogen KA, Estes NA 3rd, Freedman RA, Gettes LS, Gillinov AM, Gregoratos G, Hammill SC, Hayes DL, Hlatky MA, Newby LK, Page RL, Schoenfeld MH, Silka MJ, Stevenson LW, Sweeney MO, Tracy CM, Epstein AE, Darbar D, DiMarco JP, Dunbar SB,

Author Manuscript Author Manuscript Author Manuscript Author Manuscript

Estes NA 3rd, Ferguson TB Jr, Hammill SC, Karasik PE, Link MS, Marine JE, Schoenfeld MH, Shanker AJ, Silka MJ, Stevenson LW, Stevenson WG, Varosy PD. American College of Cardiology F, American Heart Association Task Force on Practice G Heart Rhythm S. 2012 ACCF/AHA/HRS focused update incorporated into the ACCF/AHA/HRS 2008 guidelines for device-based therapy of cardiac rhythm abnormalities: a report of the American College of Cardiology Foundation/ American Heart Association Task Force on Practice Guidelines and the Heart Rhythm Society. J Am Coll Cardiol. 2013; 61:e6–75. [PubMed: 23265327]

2. Epstein AE, DiMarco JP, Ellenbogen KA, Estes NA III, Freedman RA, Gettes LS, Gillinov AM, Gregoratos G, Hammill SC, Hayes DL, Hlatky MA, Newby LK, Page RL, Schoenfeld MH, Silka MJ, Stevenson LW, Sweeney MO. ACC/AHA/HRS 2008 guidelines for Device-Based Therapy of Cardiac Rhythm Abnormalities: executive summary. Heart Rhythm. 2008; 5:934–955. [PubMed: 18534377]
3. Buxton AE, Lee KL, Hafley GE, Pires LA, Fisher JD, Gold MR, Josephson ME, Lehmann MH, Prystowsky EN. Limitations of ejection fraction for prediction of sudden death risk in patients with coronary artery disease: lessons from the MUSTT study. J Am Coll Cardiol. 2007; 50:1150–1157. [PubMed: 17868806]
4. Lee DS, Krahn AD, Healey JS, Birnie D, Crystal E, Dorian P, Simpson CS, Khaykin Y, Cameron D, Janmohamed A, Yee R, Austin PC, Chen Z, Hardy J, Tu JV. Evaluation of early complications related to De Novo cardioverter defibrillator implantation insights from the Ontario ICD database. J Am Coll Cardiol. 2010; 55:774–782. [PubMed: 20170816]
5. Reddy VY, Reynolds MR, Neuzil P, Richardson AW, Taborsky M, Jongnarangsin K, Kralovec S, Sediva L, Ruskin JN, Josephson ME. Prophylactic catheter ablation for the prevention of defibrillator therapy. NEnglJ Med. 2007; 357:2657–2665.
6. Kuck KH, Schaumann A, Eckardt L, Willems S, Ventura R, Delacretaz E, Pitschner HF, Kautzner J, Schumacher B, Hansen PS. group Vs. Catheter ablation of stable ventricular tachycardia before defibrillator implantation in patients with coronary heart disease (VTACH): a multicentre randomised controlled trial. Lancet. 2010; 375:31–40. [PubMed: 20109864]
7. Ghanbari H, Baser K, Yokokawa M, Stevenson W, Della Bella P, Vergara P, Deneke T, Kuck KH, Kottkamp H, Fei S, Morady F, Bogun F. Noninducibility in postinfarction ventricular tachycardia as an end point for ventricular tachycardia ablation and its effects on outcomes: a meta-analysis. Circ Arrhythm Electrophysiol. 2014; 7:677–83. [PubMed: 24879789]
8. Couderc JP, Xiaojuan X, Zareba W, Moss AJ. Assessment of the stability of the individual-based correction of QT interval for heart rate. AnnNoninvasiveElectrocardiol. 2005; 10:25–34.
9. Couderc JP. The telemetric and Holter ECG warehouse initiative (THEW): a data repository for the design, implementation and validation of ECG-related technologies. ConfProcIEEE Eng MedBiolSoc. 2010; 2010:6252–6255.
10. Tereshchenko LG, Cygankiewicz I, McNitt S, Vazquez R, Bayes-Genis A, Han L, Sur S, Couderc JP, Berger RD, de Luna AB, Zareba W. Predictive value of beat-to-beat QT variability index across the continuum of left ventricular dysfunction: competing risks of noncardiac or cardiovascular death and sudden or nonsudden cardiac death. Circ Arrhythm Electrophysiol. 2012; 5:719–27. [PubMed: 22730411]
11. Sur S, Han L, Tereshchenko LG. Comparison of sum absolute QRST integral, and temporal variability in depolarization and repolarization, measured by dynamic vectorcardiography approach, in healthy men and women. PLoS One. 2013; 8:e57175. [PubMed: 23451181]
12. Edenbrandt L, Pahlm O. Vectorcardiogram synthesized from a 12-lead ECG: superiority of the inverse Dower matrix. JElectrocardiol. 1988; 21:361–367.
13. Sornmo L. Vectorcardiographic loop alignment and morphologic beat-to-beat variability. IEEE transactions on bio-medical engineering. 1998; 45:1401–13. [PubMed: 9835189]
14. Astrom M, Carro Santos E, Sornmo L, Laguna P, Wohlfart B. Vectorcardiographic loop alignment and the measurement of morphologic beat-to-beat variability in noisy signals. IEEE transactions on bio-medical engineering. 2000; 47:497–506. [PubMed: 10763295]
15. Josephson, ME. Clinical cardiac electrophysiology : techniques and interpretations. 4. Philadelphia: Wolters Kluwer/Lippincott Williams & Wilkins, Health; 2008.
16. Simson MB, Untereker WJ, Spielman SR, Horowitz LN, Marcus NH, Falcone RA, Harken AH, Josephson ME. Relation between late potentials on the body surface and directly recorded

Author Manuscript Author Manuscript Author Manuscript Author Manuscript

fragmented electrograms in patients with ventricular tachycardia. Am J Cardiol. 1983; 51:105–112. [PubMed: 6849248]

17. Savard P, Rouleau JL, Ferguson J, Poitras N, Morel P, Davies RF, Stewart DJ, Talajic M, Gardner M, Dupuis R, Lauzon C, Sussex B, Potvin L, Warnica W. Risk stratification after myocardial infarction using signal-averaged electrocardiographic criteria adjusted for sex, age, and myocardial infarction location. Circulation. 1997; 96:202–13. [PubMed: 9236435]
18. Gomes JA, Cain ME, Buxton AE, Josephson ME, Lee KL, Hafley GE. Prediction of long-term outcomes by signal-averaged electrocardiography in patients with unsustained ventricular tachycardia, coronary artery disease, and left ventricular dysfunction. Circulation. 2001; 104:436–441. [PubMed: 11468206]
19. Cain ME, Arthur RM, Trobaugh JW. Detection of the fingerprint of the electrophysiological abnormalities that increase vulnerability to life-threatening ventricular arrhythmias. J IntervCard Electrophysiol. 2003; 9:103–118.
20. Lander P, Gomis P, Goyal R, Berbari EJ, Caminal P, Lazzara R, Steinberg JS. Analysis of abnormal intra-QRS potentials. Improved predictive value for arrhythmic events with the signal-averaged electrocardiogram. Circulation. 1997; 95:1386–1393. [PubMed: 9118504]
21. Gomis P, Jones DL, Caminal P, Berbari EJ, Lander P. Analysis of abnormal signals within the QRS complex of the high-resolution electrocardiogram. IEEE TransBiomedEng. 1997; 44:681–693.
22. Nearing BD, Wellenius GA, Mittleman MA, Josephson ME, Burger AJ, Verrier RL. Crescendo in depolarization and repolarization heterogeneity heralds development of ventricular tachycardia in hospitalized patients with decompensated heart failure. Circ Arrhythm Electrophysiol. 2012; 5:84–90. [PubMed: 22157521]
23. de JS, van Veen TA, van Rijen HV, de Bakker JM. Fibrosis and cardiac arrhythmias. J CardiovascPharmacol. 2011; 57:630–638.

Author Manuscript Author Manuscript Author Manuscript Author Manuscript

Highlights

- Novel method to study ventricular conduction on surface ECG is presented
- Speed, curvature, orbital frequency, planarity of filtered VCG loops was measured
- Electrophysiology of post-infarct ventricular tachycardia was charactrized

Author Manuscript Author Manuscript Author Manuscript Author Manuscript

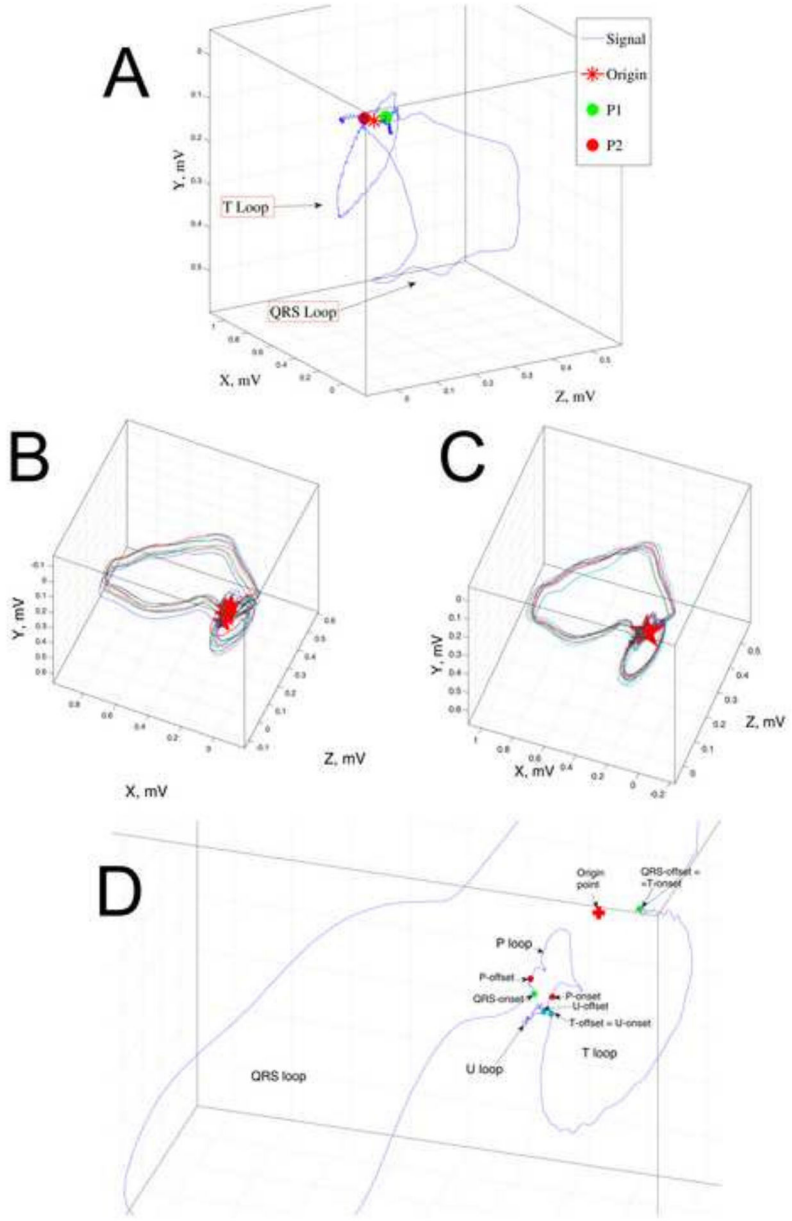

Figure 1.

A. Detection of the origin-point of the VCG loop representing a single sinus heartbeat. An unfiltered VCG from a patient with prior MI and MMVT is shown. Points P1 and P2 (green and red circles) are detected as the 2 points closest in three-dimensional space and distant in time during a single heartbeat. The origin-point (star) is defined as the point halfway along a line connecting P1 and P2. **B.** Removal of respiration effects. Original "raw" presentation of 11 consecutive sinus beats: multiple VCG loops of different size are presented in different locations and different planes in three-dimensional space. The origin points of each beat (stars) are located separately from each other. **C**. After respiration removal: loops are translocated, rotated, and re-scaled. **D**. Detection of the onset and offset of VCG loops. Onset and offset of the P, QRS, T, and U loops are marked by colored circles.

Author Manuscript Author Manuscript Author Manuscript Author Manuscript

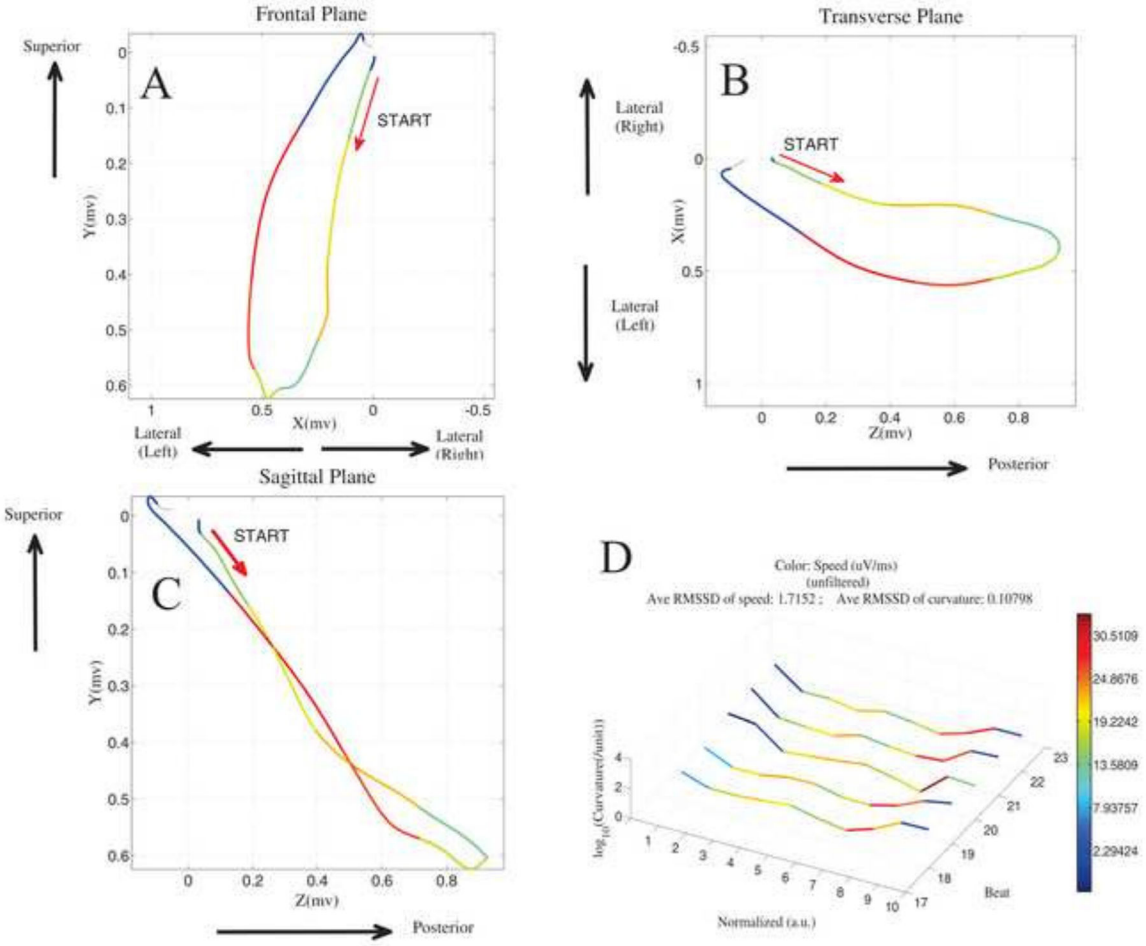

Figure 2.

The velocity and curvature of the heart vector movement through the QRS loop. Unfiltered sinus rhythm VCG loop from a MMVT patient is shown. Frontal (**A**), horizontal (**B**), and sagittal (**C**) planes are shown, with the color of each segment representing speed (purple = slowest; red=fastest). **D.** 5 consecutive sinus beats are plotted. The x-axis shows 10 normalized time segments from the onset of the QRS loop. The y-axis shows $\log_{10}$-transformed curvature. The z- axis shows the order of consecutive beats (1–5). The speed color scale is computed automatically using the minimum and maximum data values as shown by the legend.

Author Manuscript
Author Manuscript
Author Manuscript
Author Manuscript

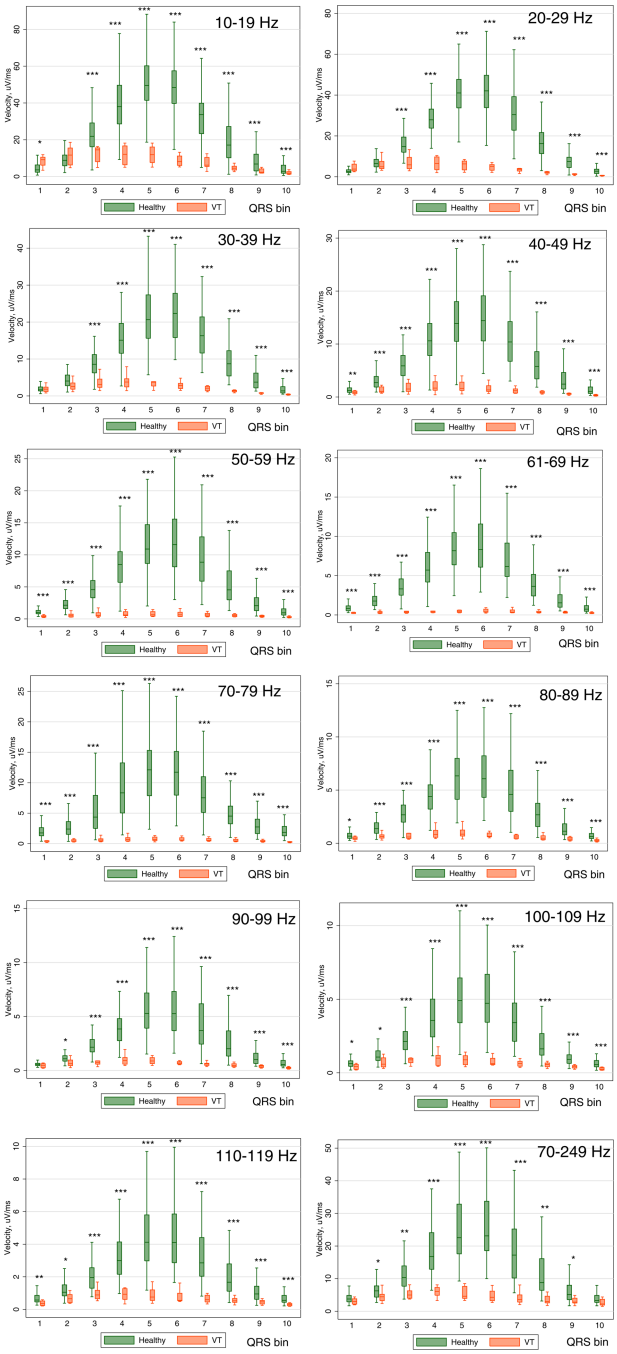

Figure 3.

Boxplots of normalized speed of the QRS vector in healthy controls and patients with infarct cardiomyopathy and ventricular tachycardia (VT cases). Median (*horizontal line crossing the box*) and interquartile range [IQR] (*box*) of spatial QRS speed is shown. Whiskers specify the adjacent values, defined as the most extreme values within 1.5 IQR of the nearer quartile. *=P<0.05; **=P<0.001; ***=P<0.0001

Author Manuscript
Author Manuscript
Author Manuscript
Author Manuscript

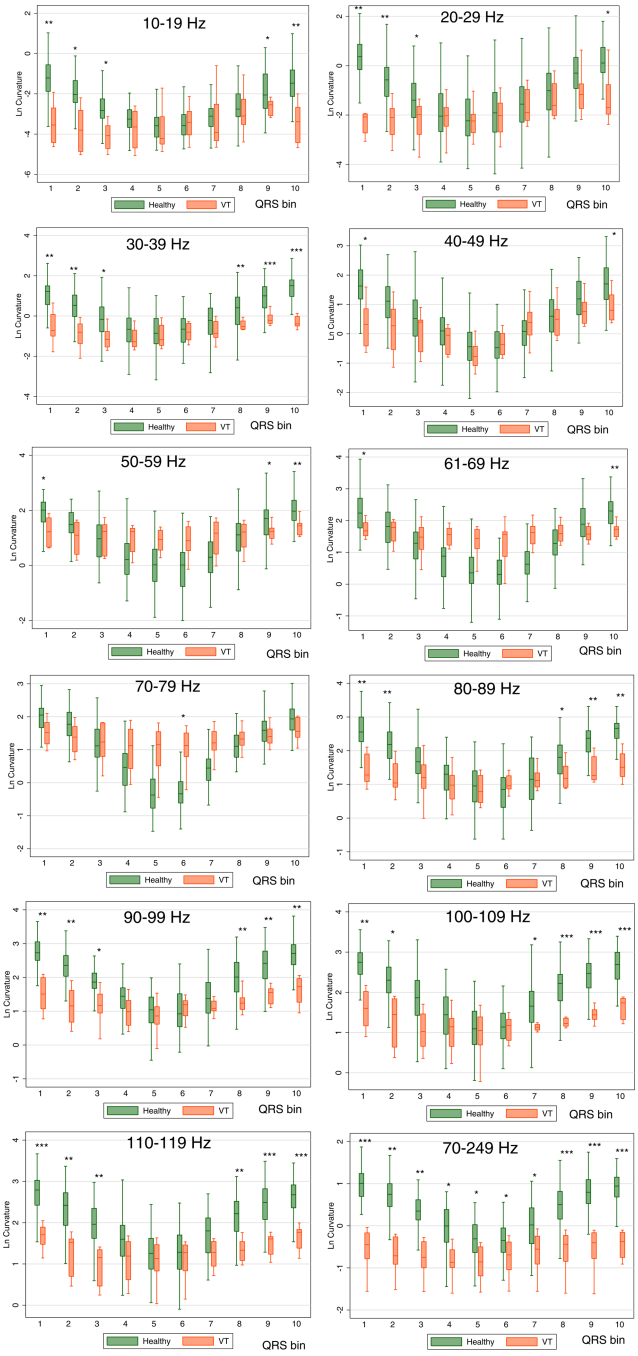

Figure 4.

Boxplots of normalized log-transformed curvature of the QRS loop in healthy controls and patients with infarct cardiomyopathy and ventricular tachycardia (VT cases). Median (*horizontal line crossing the box*) and interquartile range [IQR] (*box*) of QRS loop curvature is shown. Whiskers specify the adjacent values, defined as the most extreme values within 1.5 IQR of the nearer quartile. *=P<0.05; **=P<0.001; ***=P<0.0001

Author Manuscript Author Manuscript Author Manuscript Author Manuscript

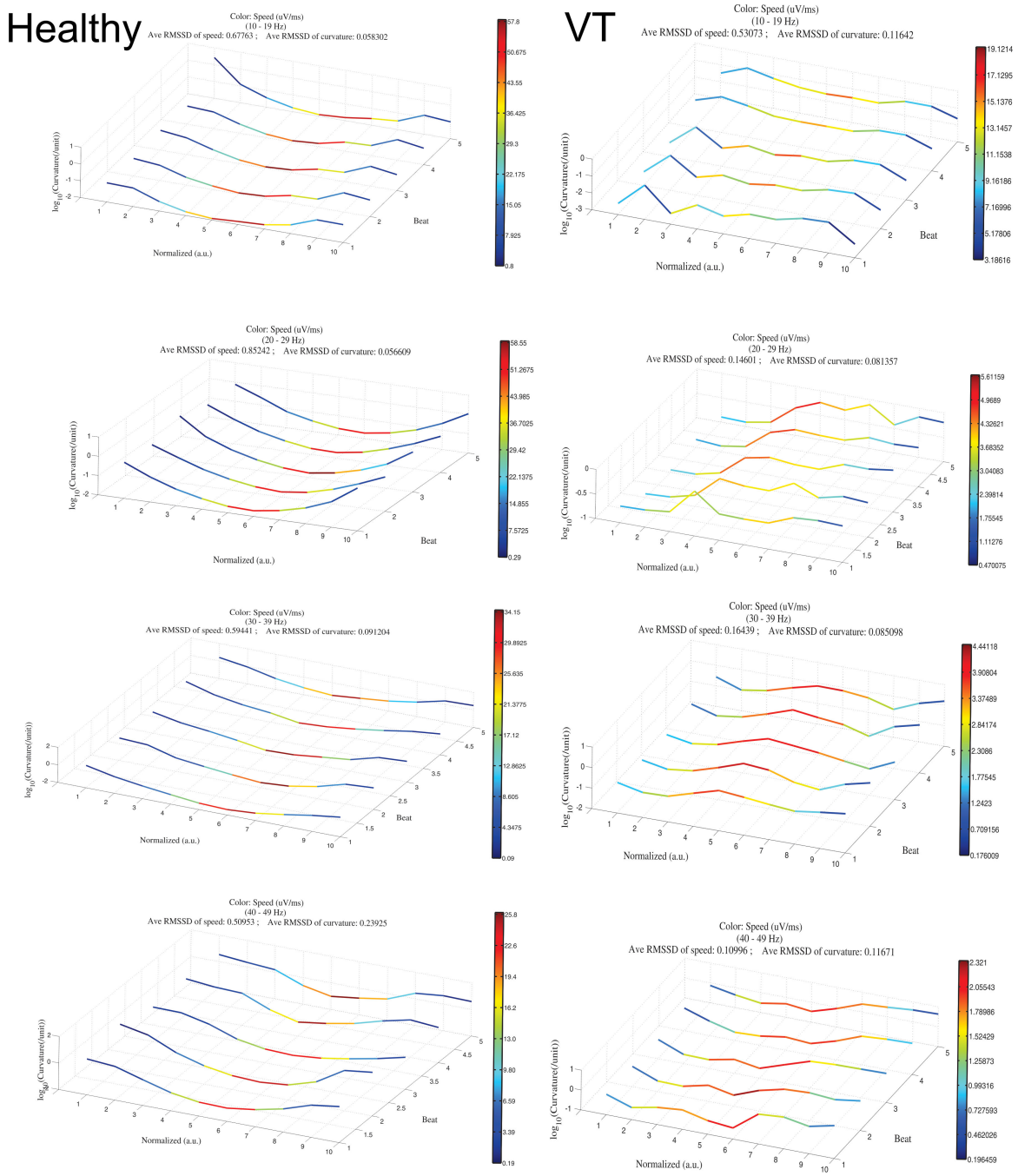

Figure 5.

Comparison of the speed and curvature of filtered heart vector movement throughout the QRS in sinus rhythm in healthy subject (left column) and a patient with MMVT (right column). QRS loops filtered at 10–19Hz, 20–29Hz, 30–39Hz, and 40–49Hz are shown in rows 1–4, respectively. The x-axis shows 10 normalized time segments from the onset of the QRS loop. The y-axis shows $\log_{10}$-transformed curvature. The z- axis shows the order of consecutive beats (1–5). The color scale represents speed and is computed using the

minimum and maximum velocity values as shown by the legend on each small panel (purple = minimum speed; red = maximum speed).

Author Manuscript Author Manuscript Author Manuscript Author Manuscript

Author Manuscript Author Manuscript Author Manuscript Author Manuscript

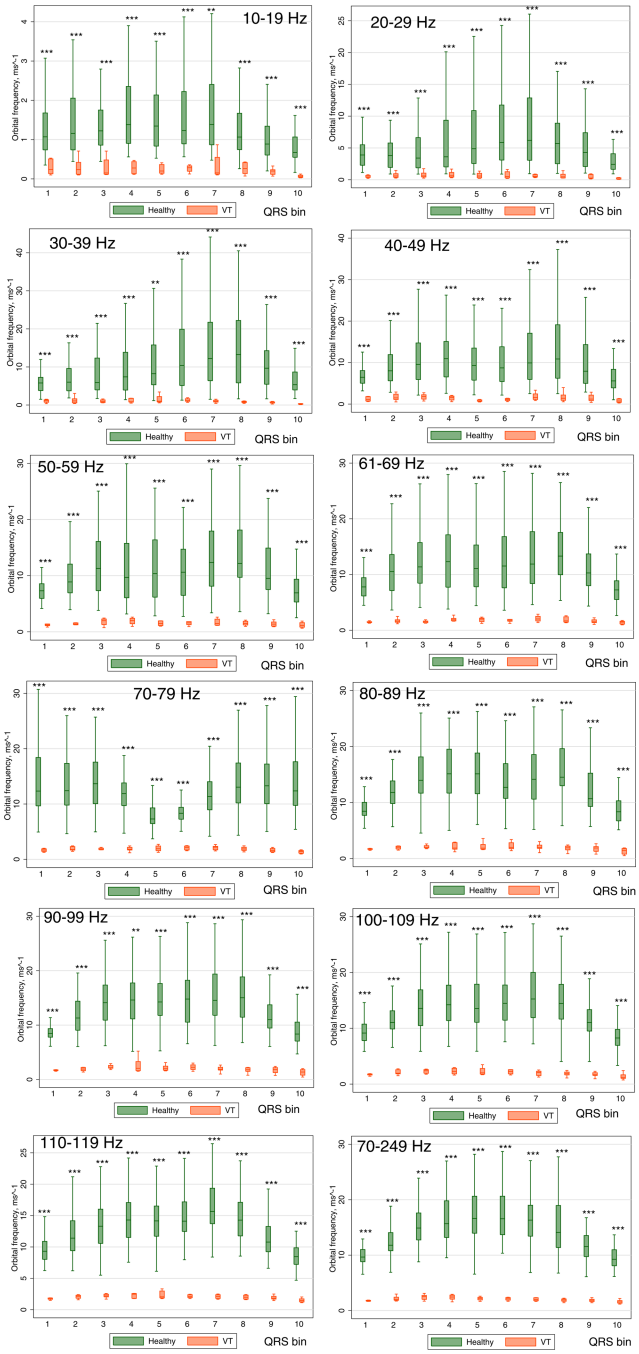

Figure 6.

Boxplots of normalized orbital frequency Ω of the spatial QRS vector movement in Healthy controls and patients with infarct cardiomyopathy and ventricular tachycardia (VT cases). Median (*horizontal line crossing the box*) and interquartile range [IQR] (*box*) of orbital frequency is shown. Whiskers specify the adjacent values, defined as the most extreme values within 1.5 IQR of the nearer quartile. *=P<0.05; **=P<0.001; ***=P<0.0001

Author Manuscript Author Manuscript Author Manuscript Author Manuscript

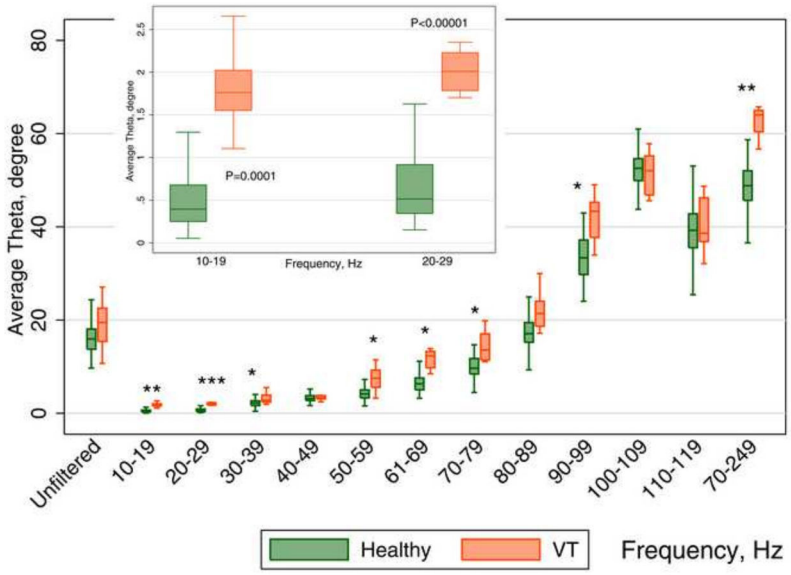

Figure 7.

Boxplots of the planarity angle θ of the QRS loop in Healthy controls and patients with infarct cardiomyopathy and ventricular tachycardia (VT cases). Median (*horizontal line crossing the box*) and interquartile range [IQR] (*box*) of QRS loop planarity angle is shown. Whiskers specify the adjacent values, defined as the most extreme values within 1.5 IQR of the nearer quartile. *=P<0.05; **=P<0.001; ***=P<0.0001

Author Manuscript Author Manuscript Author Manuscript Author Manuscript

Table 1

Results of the nonparametric receiver operating characteristic (ROC) analyses for prediction of outcome (healthy vs. VT cases). The area under the ROC curve (AUC) with 95% confidence inteval.

	Velocity, μV/ms		Curvature, $μV^{-1}$		Orbital frequency, ms^{-1}		Planarity, °	
Frequency, Hz	**ROC AUC**	**95%CI**	**ROC AUC**	**95%CI**	**ROC AUC**	**95%CI**	**ROC AUC**	**95%CI**
unfiltered	0.923	0.900–0.946	0.503	0.436–0.569	0.965	0.948–0.982	0.698	0.443–0.952
10–19	0.731	0.693–0.769	0.725	0.666–0.784	0.957	0.930–0.983	0.966	0.930–1.00
20–29	0.824	0.791–0.857	0.695	0.648–0.743	0.975	0.962–0.988	0.951	0.907–0.995
30–39	0.836	0.804–0.869	0.743	0.701–0.782	0.986	0.976–0.996	0.770	0.604–0.937
40–49	0.878	0.850–0.906	0.618	0.564–0.672	0.995	0.990–0.999	0.588	0.395–0.781
50–59	0.950	0.932–0.967	0.477	0.431–0.523	0.9995	0.999–1.00	0.818	0.603–1.00
61–69	0.966	0.953–0.980	0.593	0.551–0.635	1.00	0.9999–1.00	0.969	0.928–1.00
70–79	0.979	0.969–0.989	0.579	0.532–0.626	0.999	0.997–1.00	0.860	0.753–0.966
80–89	0.877	0.849–0.905	0.698	0.655–0.741	0.9999	0.9998–1.00	0.747	0.517–0.977
90–99	0.846	0.814–0.878	0.747	0.707–0.786	1.00	0.9999–1.00	0.806	0.561–1.00
100–109	0.848	0.816–0.881	0.772	0.736–0.809	0.9997	0.9992–1.00	0.437	0.163–0.711
110–119	0.850	0.816–0.883	0.795	0.760–0.830	0.9999	0.9998–1.00	0.556	0.323–0.788
70–249	0.813	0.777–0.849	0.889	0.863–0.914	1.00	0.9999–1.00	0.995	0.985–1.00